Evaluation of silica-supported metal and metal phosphide nanoparticle catalysts for the hydrodeoxygenation of guaiacol under *ex-situ* catalytic fast pyrolysis conditions

Michael B. Griffin[a], Frederick G. Baddour[b], Susan E. Habas[a], Daniel A. Ruddy[b], Joshua A. Schaidle*[a]

[a]*National Bioenergy Center, National Renewable Energy Laboratory, 15013 Denver West Pkwy, Golden, CO, USA*
[b]*Chemistry and Nanoscience Center, National Renewable Energy Laboratory, 15013 Denver West Pkwy, Golden, CO, USA*
**Email: Joshua.Schaidle@nrel.gov; Fax: 1-303-384-7951; Phone: 1-303-384-7823*

Abstract:

A series of metal and metal phosphide catalysts were investigated for the hydrodeoxygenation of guaiacol under *ex-situ* catalytic fast pyrolysis (CFP) conditions (350 °C, 0.5 MPa, 12 H_2:1 guaiacol, weight hourly space velocity 5 h^{-1}). Ligand-capped Ni, Pt, Rh, Ni_2P, and Rh_2P nanoparticles (NPs) were prepared using solution-phase synthesis techniques and dispersed on a silica support. For the metal phosphide NP-catalysts, a synthetic route that relies on the decomposition of a single molecular precursor was employed. The reactivity of the NP-catalysts was compared to a series of reference materials including Ni/SiO_2 and Pt/SiO_2 prepared using incipient wetness (IW) impregnation and a commercial (com) Pt/SiO_2 catalyst. The NP-Ni/SiO_2 catalyst exhibited the largest reduction in the oxygen mol% of the organic phase and outperformed the IW-Ni/SiO_2 material. Although it was less active for guaiacol conversion than NP-Ni/SiO_2, NP-Rh_2P/SiO_2 demonstrated the largest production of completely deoxygenated products and the highest selectivity to anisole and benzene, suggesting that it is a promising catalyst for deoxygenation of aryl-OH bonds. The com-Pt/SiO_2 and IW-Pt/SiO_2 catalyst exhibited the highest normalized rate of guaiacol conversion per m^2 and per gram of active phase, respectively, but did not produce any completely deoxygenated products.

Key Words:

Guaiacol, bio-oil, catalytic fast pyrolysis, deoxygenation, metal phosphide, nanoparticle, ligand

1. Introduction

Biomass derived liquid fuels have the potential to provide a renewable, carbon-neutral energy source that is compatible with current infrastructure and can be realized on a relatively short time scale [1]. This is particularly important for the heavy vehicle transportation sector, where the utilization of electric and hybrid technologies remains difficult. One route for the production of biomass derived fuels is fast pyrolysis, which can occur at mild temperatures (480-520 °C) and forms a liquid bio-oil product [2-5]. While bio-oil has the potential to supplement crude-oil, there are major chemical differences between these two materials, and bio-oil must be upgraded before it is suitable for use as a drop-in liquid hydrocarbon feedstock [1]. Of primary concern is the high oxygen content of bio-oil, which contributes to a number of undesirable characteristics including low heating value, chemical instability, and high viscosity [6]. Therefore, deoxygenation is critical to enabling transportation fuel production from biomass pyrolysis at the industrial scale. One option for bio-oil deoxygenation is *ex-situ* catalytic fast pyrolysis (CFP) in which the pyrolysis vapors are catalytically deoxygenated external to the pyrolysis reactor, but prior to condensation (Figure 1) [1,7,8].

Acidic catalysts such as zeolites have been investigated under *ex-situ* CFP conditions and exhibit promising performance, but are prone to rapid deactivation due to carbonaceous deposits [5]. Transition metal sulfides have also been considered, but require significant hydrogen pressure (5-20 MPa) and the addition of H_2S to maintain activity [1]. A preferred catalyst would readily activate H_2 and exhibit superior stability when exposed to the high temperature, low pressure, high-steam, and near-stoichiometric H_2 conditions that occur during *ex-situ* CFP [1]. Recent research activities using bio-oil model compounds have identified a number of promising materials including noble metal, base metal, and metal phosphide catalysts [9-19]. Metal phosphides have been shown to exhibit hydrotreating activities similar to, or better than, transition metal sulfide-based materials and noble metals [17]. They are capable of activating H_2 and possess bifunctional catalytic properties that result from a combination of metallic and acidic surface sites [18]. These attributes suggest that metal phosphide catalysts may be excellent candidates for *ex-situ* CFP, particularly when coupled with tunable electronic structure and surface metal site density based on the choice of transition metal and metal-to-phosphorus ratio [19]. Bulk-scale, temperature programmed reduction and commercial synthesis methods such as incipient wetness impregnation (IW) have been commonly used to prepare catalytic materials for bio-oil deoxygenation [13,9-12,14]. However, significant advances in the solution-phase synthesis of nanoparticles (NPs) have enabled an increased level of control over the size, shape, and composition of catalytic particles [20,21].

Herein we report the results of an investigation into guaiacol hydrodeoxygenation over silica-supported Ni, Pt, Rh, Ni_2P, and Rh_2P NP-catalysts. The performance of these catalysts was compared to a series of reference materials including IW-Pt/SiO_2, IW-Ni/SiO_2, and a commercial (com) Pt/SiO_2 catalyst. Silica was selected as a relatively inert support in order to focus on the performance of the active phase while minimizing the effects of the supporting material. Guaiacol was selected as a model compound to represent the substituted phenolics that are present in lignin-derived bio-oil, and its multiple functional groups make it an ideal model compound to better understand the fundamental chemical transformations that take place during bio-oil deoxygenation [10]. The metrics used to assess guaiacol upgrading include the rate of guaiacol conversion, the extent of deoxygenation, and the extent of hydrogenation. The catalytic investigation reported herein offers insight into the use of solution-phase synthetic methods, examines the differences in reactivity between metal and metal phosphide catalysts, and presents the first investigation into Rh_2P for the deoxygenation of bio-oil model compounds under *ex-situ* CFP conditions.

2. Experimental

2.1 Materials

Metal reagents $Ni(CO)_2(PPh_3)_2$, $RhCl(CO)(PPh_3)_2$, $Pt(acac)_2$, and $Pt(NH_3)_4(NO_3)_2$ were purchased from Strem Chemicals. Phosphate reagents, $(NH_4)H_2PO_4$ and $(NH_4)_2HPO_4$, were obtained from JT Baker. All solvents and reagents were used as received unless otherwise noted. The silica support, Sipernat-22, was provided by Evonik and calcined at 600 °C in flowing air prior to use. The BET surface area of the calcined silica was measured as 190 $m^2\ g^{-1}$, and the aqueous IW point was determined to be 3.9 mL g^{-1}. Crushed quartz (150-250 and 300-425 micron, Powder Technologies Inc.) and silicon carbide (177-250 micron, McMaster Carr) were used as diluent materials for reactor testing. Guaiacol (>98%) was obtained from Sigma-Aldrich, and acetone (HPLC grade) was obtained from Fisher Scientific. Certified gas blends (5% argon/95% hydrogen and 1% oxygen/99% helium) were obtained from Air Liquide. Hydrogen (UHP, General Air), argon (UHP, General Air), and nitrogen (house supply) were also utilized. The commercial 5 wt% Pt/SiO_2 catalyst was purchased from Strem Chemicals and was reduced *in-situ* at 450 °C in flowing hydrogen prior to reaction [22].

2.2 Catalyst synthesis

2.2.1 Solution-phase metal nanoparticle syntheses

The Pt NPs were prepared based on a method by Z. Liu, et al. [23]. Briefly, 0.190 g $Pt(acac)_2$, 0.780 g 1,2-hexadecanediol and 40 mL diphenyl ether were heated to 110 °C at a rate of 5 °C min^{-1} under a N_2 atmosphere. The solution was held at 110 °C for 2 min, during which time 0.34 mL of oleylamine (OAm) was added dropwise. The solution was heated to 175 °C at 5 °C min^{-1} and held at temperature for 1 h. The heat source was removed and the reaction mixture allowed to cool naturally. Once cool, 40 mL of ethanol was added, and the suspension was sonicated for 5 min. The NPs were then recovered by centrifugation.

The Ni NPs were prepared as described by S. Carenco, et al. [24]. Briefly, 2.0 g $Ni(acac)_2$, 25.6 mL OAm, and 2 mL octadecene (ODE) were heated at 100 °C under vacuum for 1 h. After refilling with a N_2 atmosphere, 1.74 mL trioctylphosphine was added and the solution heated rapidly to 220 °C and held at temperature for 2 h. The resulting NP suspension was cooled and 40 mL acetone was added, followed by recovery of the NPs by centrifugation.

The Rh NPs were prepared based on a procedure by K. H. Park, et al. [25]. Briefly, $Rh(acac)_2$ (0.100 g, 0.24 mmol) and 4 mL of dried OAm were heated to 100 °C. This solution was rapidly injected into dried OAm (6 mL) at 250 °C under a N_2 atmosphere. The solution was held at this temperature for 1 h. After cooling to room temperature, the NP suspension was precipitated with 10 mL methanol and separated by centrifugation. The NPs were washed once with $CHCl_3$/methanol.

2.2.2 Solution-phase metal phosphide nanoparticle syntheses

A single-source molecular precursor route was utilized to prepare the metal phosphide NPs [26]. The Ni_2P NPs were prepared using a mixture of $Ni(PPh_3)_2(CO)_2$ (0.639 g, 1.0 mmol) and PPh_3 (1.049 g, 4.0 mmol) in dry OAm (6.6 mL, 20.0 mmol) and ODE (6 mL). The reaction mixture was maintained under an N_2 atmosphere and heated to 320 °C in ca. 15 min. The temperature was held at 320 °C for 2 h, after which time the heat source was removed, and the resulting black suspension was allowed to cool naturally. Approximately 15 mL of 2-propanol was added to the reaction mixture to flocculate the particles, which were then separated by centrifugation.

The Rh_2P NPs were prepared using a mixture of $Rh(PPh_3)_2(CO)Cl$ (0.69 g, 1.0 mmol), OAm (4.9 mL, 15.0 mmol), and ODE (8.0 mL), which was heated to 100 °C under vacuum. After 1 h, the reaction mixture was heated to 300 °C under N_2 in ca. 15 min. The temperature was held at 300 °C for 1 h, after which time the heat source was removed, and the resulting suspension was allowed to cool naturally. Approximately 5 mL of $CHCl_3$ was added to the mixture followed by approximately 15 mL of 2-propanol to precipitate the particles. The NPs were separated by centrifugation.

2.2.3 Nanoparticle supporting procedure

The recovered NPs were redispersed in 10 mL of $CHCl_3$ and added dropwise to a suspension of the silica support in $CHCl_3$ (1 g mL^{-1}), in order to yield a catalyst with 5 wt% metal or metal phosphide loading. The mixture was sonicated for 5 min and stirred at room temperature overnight. The resulting catalyst was separated via centrifugation, dried *in vacuo*, and stored under an Ar atmosphere.

2.2.4 Incipient wetness impregnation catalyst syntheses

Silica-supported Pt and Ni were prepared from their respective metal precursors via standard IW methods. Briefly, 18 mL of an aqueous solution of $Pt(NH_3)_4(NO_3)_2$ or $Ni(NO_3)_2 \cdot 6H_2O$ corresponding to a 5.0 wt% metal loading was added dropwise to 4.75 g of silica support. The impregnated material was dried at 50 °C overnight in an oven and reduced in the reactor at 450 °C in flowing H_2 prior to reaction testing.

2.3 Catalyst characterization

Powder X-ray diffraction (XRD) data were collected using a Rigaku Ultima IV diffractometer with a Cu Kα source (40 kV, 44 mA). Diffraction patterns were collected in the 2θ range of 20–80 degrees at a scan rate of 4 ° min^{-1}. Samples (10–20 mg) were supported on a glass sample holder with a 0.2 mm recessed sample area and were pressed into the recession with a glass slide to obtain a uniform z-axis height. Data were compared to reference card files from the International Center for Diffraction Data (Ni: 00-004-0850, Ni_2P: 01-074-1385, Pt: 00-004-0802, Rh: 01-087-0714, Rh_2P: 01-071-6466) to confirm the identity and phase of the sample. The crystallite sizes were estimated from XRD peak broadening of the supported catalysts using the Scherrer equation. Samples for transmission electron microscopy (TEM) were dropcast onto carbon-coated copper grids (Ted Pella part no. 01824) from chloroform or hexanes suspensions. Imaging was performed using a FEI G20 Tecnai operating at 200 keV. Elemental analysis was performed by Galbraith Laboratories (Knoxville, TN) using inductively coupled plasma optical emission spectroscopy (ICP-OES).

No effort was made to remove the stabilizing ligands on the surface of the NP-catalysts prior to reaction. Instead, the catalysts were activated in the reactant mixture using a slow temperature ramp. Due to the uncertainty in ligand coverage, especially at reaction conditions, chemical titration methods (e.g., H_2 or CO chemisorption) may not provide an accurate measurement of accessible active sites and could convolute a direct site comparison between catalysts prepared by IW and solution-phase techniques. As an alternative, the active phase surface area for each catalyst was determined by analysis of TEM images. The particle size distributions were obtained by the manual measurement of >100 particles for the IW-Ni/SiO_2, IW-Pt/SiO_2, com-Pt/SiO_2, and NP-Rh/SiO_2 catalysts or by an automated calculation conducted by ImageJ for the unsupported Ni, Ni_2P, Rh_2P, and Pt NPs. Active phase-support wetting properties were not assessed in this study, thus calculations were performed based on particle shapes, as determined by TEM, with no correction for surface wetting. The active phase surface area per gram of catalyst was calculated according to Eq. 1 from the active phase wt% (determined by ICP-OES), active phase density, and active phase particle shape and size distribution (determined by TEM).

Eq. 1: Active phase surface area per gram of catalyst $= \left(\frac{\sum_{i=1}^{n} \frac{SA_i}{V_i}}{n} \right) \text{x } \frac{wt\%}{\rho \, x \, 100}$

(SA_i) = surface area of active phase particle i
(V_i) = volume of active phase particle i
$(wt\%)$ = active phase weight percent
ρ = active phase density
n = number of particles counted

2.4 Guaiacol deoxygenation under *ex-situ* CFP conditions

Approximately 300 – 500 mg of each catalyst was physically mixed with 177-250 µm particles of SiC (1:2 catalyst:SiC by mass) and loaded into the isothermal zone of a 20 mL downward-flow tubular packed bed reactor. The temperature of the 4 mL isothermal zone was monitored using a 4-point thermocouple inserted into the catalyst bed. Typical temperature variation was within ±1 °C of the set point. Approximately 2 mL of 150-250 µm crushed quartz was added to each side of the catalyst bed, and the remainder of the reactor was packed with 300-425 µm crushed quartz. The reaction conditions were selected in order to investigate catalytic performance in a parameter space relevant to ex-situ CFP, which occurs at higher temperature and lower hydrogen partial pressure than other upgrading techniques such as hydrotreating [1].To begin an experiment, the temperature of the isothermal zone was increased to 250 °C in flowing nitrogen. At this point, guaiacol was introduced from an Eldex Optos 1LMP HPLC pump and vaporized into a stream of hydrogen (95%) and argon (5%). The catalyst was exposed to a vapor stream consisting of 88 mol% hydrogen, 5 mol% argon, and 7 mol% guaiacol flowing at a WHSV of 10 h^{-1} (in terms of guaiacol flowrate and catalyst mass). Next, the reactor was pressurized to 0.5 MPa, and the temperature was increased from 250 °C to 350 °C at 3 °C min^{-1}. Once the isothermal zone of the reactor was stable at 350 °C, the WHSV was decreased to 5 h^{-1}. A 12:1 molar ratio of H_2:guaiacol was maintained for the duration of the 8 h reaction period.

Condensable products from the reaction were collected in a hot trap controlled at 80 °C. These products were removed from the trap hourly and analyzed using an Agilent Technologies 7890A gas chromatograph equipped with a flame ionization detector (FID) and mass spectrometer. Uncondensed products in the gas phase were analyzed online using a separate Agilent Technologies 7890B gas chromatograph modified by Wasson ECE Instrumentation. Products were identified through retention time comparison with known standards and confirmed using mass spectrometry. Quantitative analysis was carried out on both systems using a flame ionization detector, which had been calibrated with standards of known concentrations. In the event that a standard was unavailable, response factors were extrapolated from similar compounds based on carbon number. Argon was used as an internal standard for the gas phase analysis and all values were adjusted to account for changes in total molar flow rate. Analysis of the condensed products was carried out by determining the molar composition and formula weight from gas chromatography and measuring the mass flow rate by dividing the sample mass by the collection time. Using the mass flow rate and formula weight, the total molar flow rate of the condensed phase was calculated. From the total molar flow rate and the molar composition, the individual molar flow rate of each product was determined. An experiment carried out at a WHSV of 10 h^{-1} using SiO_2 in the absence of an active phase exhibited 24% conversion and a negligible reduction in the oxygen mol% of the organic phase (12%). In all experiments, the mass balances were between 78-94%. Although they are not quantified in this study, carbon deposition on the catalyst bed as well as liquid hold-up in the condensation system are thought to be the primary contributors to mass balance deviations. To check for the absence of external and internal mass transfer limitations, the Weisz-Prater and Mears' criterion were calculated. The resulting values were significantly below 0.1, indicating that mass transfer limitations did

not affect the observed reaction rates. In order to assess the error associated with the values reported in this study, a set of experiments was carried out in triplicate over NP-Ni/SiO_2 under *ex-situ* CFP conditions (350 °C, 0.5 MPa, 12:1 H_2:guaiacol, WHSV 10 h^{-1}). The average guaiacol conversion and H/C ratio of the organic phase products were found to be 76 ± 4.2% and 1.3 ± 0.016 respectively. In both cases, the standard deviation represented < 6% of the average.

Guaiacol conversion was calculated according to Eq. 2 and is defined as the percent decrease in the molar flow rate of guaiacol between the feed and outlet of the reactor. The rate of guaiacol conversion per m^2 of active phase was calculated according to Eq. 3 and is defined as the difference in the molar flow rate of guaiacol between the feed and outlet of the reactor divided by the total surface area of the active phase present in the reactor. The total surface area of the active phase present in the reactor was obtained by multiplying the mass of the catalyst loaded by the active phase surface area per gram of catalyst (as calculated in Eq. 1). The rate of guaiacol conversion per gram of active phase was calculated according to Eq. 4 and is defined as the difference in the molar flow rate of guaiacol between the feed and outlet of the reactor divided by the mass of the active phase present in the reactor. The mass of the active phase present in the reactor was obtained by multiplying the mass of the catalyst loaded by the active phase wt% (as determined by ICP-OES) divided by 100. The organic phase product selectivity was calculated according to Eq. 5 and is defined as the molar flow rate of an organic phase product divided by the molar flow rate of all organic phase products. Products with a carbon number ≥ 5 are considered part of the organic phase. The byproduct selectivity was calculated according to Eq. 6 and is defined as the molar flow rate of a byproduct divided by the molar flow rate of all byproducts. Products with a carbon number < 5 are considered byproducts. The H/C ratio was calculated according to Eq. 7 and is based on the molar flow rates of the products contained within the organic phase. The oxygen mol% is calculated according to Eq. 8 and is based on the molar flow rates of the entire organic phase, including unreacted guaiacol. The product yield was calculated according to Eq. 9 and is defined as the organic phase product selectivity multiplied by the guaiacol conversion. The catalytic performance of each material was compared based on data collected at 8 h time on stream (TOS). Although catalyst deactivation was not explicitly evaluated during the initial reaction period, measuring catalytic performance at 8 h TOS provides time for the effects of deactivation to influence the observed reactivity. As such, the performance of each material presented in this study is likely influenced by both intrinsic catalytic properties and stability under *ex-situ* CFP conditions. A more in-depth analysis of stability with longer reaction periods is planned for future studies.

$$\text{Eq. 2: Guaiacol conversion} = \left(\frac{[F_{Gua}]_{Feed} - [F_{Gua}]_{Outlet}}{[F_{Gua}]_{Feed}}\right) \text{x } 100$$

F_{Gua}= molar flow rate of guaiacol

$$\text{Eq. 3: Rate of guaiacol conversion per m}^2\text{ of active phase} = \left(\frac{[F_{Gua}]_{Feed} - [F_{Gua}]_{Outlet}}{g_{Cat}\, x \frac{m^2}{g_{cat}}}\right)$$

F_{Gua} = molar flow rate of guaiacol

g_{cat} = mass of catalyst loaded into reactor

$\frac{m^2}{g_{cat}}$ = active phase surface area per gram of catalyst

$$\text{Eq. 4: Rate of guaiacol conversion per gram of active phase} = \left(\frac{[F_{Gua}]_{Feed} - [F_{Gua}]_{Outlet}}{g_{Cat}\, x\, wt\%\, x \frac{1}{100}}\right)$$

F_{Gua} = molar flow rate of guaiacol

g_{cat} = mass of catalyst loaded into reactor

$wt\%$ = active phase weight percent

Eq. 5: Organic phase selectivity $= \left(\frac{(F_i)}{\sum_{i=1}^{n}(F_i)}\right) \text{x } 100$

(F_i) = molar flow rate of organic phase product i

$\sum_{i=1}^{n}(F_i)$ = total molar flow rate of organic phase products

Eq. 6: Byproduct selectivity $= \left(\frac{(F_i)}{\sum_{i=1}^{n}(F_i)}\right) \text{x } 100$

(F_i) = molar flow rate of byproduct i

$\sum_{i=1}^{n}(F_i)$ = total molar flow rate of all byproducts

Eq. 7: H/C ratio $= \left(\frac{F_H}{F_C}\right)$

F_H = molar flow rate of hydrogen in the organic phase

F_C = molar flow rate of carbon in the organic phase

Eq. 8: Oxygen mol% $= \left(\frac{F_O}{F_{Tot}}\right) \text{x } 100$

F_O = molar flow rate of oxygen in the organic phase

F_{Tot} = total molar flow rate in the organic phase

Eq. 9: Product yield $= \left(\frac{[F_{Gua}]_{Feed} - [F_{Gua}]_{Outlet}}{[F_{Gua}]_{Feed}}\right)\left(\frac{(F_i)}{\sum_{i=1}^{n}(F_i)}\right) \text{x } 100$

F_{Gua}= molar flow rate of guaiacol

(F_i) = molar flow rate of organic phase product i

$\sum_{i=1}^{n}(F_i)$ = total molar flow rate of all organic phase products

3. Results and Discussion

3.1 Catalyst characterization

The XRD patterns for all catalysts are presented in Figure 2 and confirm the phase purity of each catalyst active phase. TEM images of each catalyst are shown in Figure 3. Spherical particle geometry was observed for all materials except Rh_2P, which adopted a cubic morphology due to the anti-fluorite crystal structure [27]. In addition to spherical particles, some elongated particles were observed on IW-Pt/SiO_2 and com-Pt/SiO_2. The Ni, Pt, Rh, and Ni_2P NPs exhibit a narrow size distribution, while NP-Rh_2P/SiO_2, IW-Ni/SiO_2, IW-Pt/SiO_2, and com-Pt/SiO_2 show greater size polydispersity (Figure 4). The active phase loading, average crystallite size (XRD), average particle diameter (TEM), average particle shape, and active phase surface area are tabulated in Table 1. With the exception of NP-Ni/SiO_2 and IW-Pt/SiO_2, the average crystallite size determined from the XRD line broadening analysis was in agreement with the TEM derived average particle size. In the case of NP-Ni/SiO_2, the crystallite size as determined by XRD is significantly smaller than the average particle diameter from TEM measurements. This is consistent with the reported polycrystallinity of the prepared Ni nanoparticles [24]. For IW-Pt/SiO_2, the majority of the particles observed by TEM were less than 10 nm in diameter; however, a small population of larger particles was also apparent. This small population of larger particles has the effect of increasing the apparent average crystallite size from XRD analysis as it is a volume-weighted technique, in contrast to the number-weighted TEM analysis that favors the more numerous smaller particles.

3.2 Deoxygenation of guaiacol under *ex-situ* CFP conditions

3.2.1 Catalyst activity and product yield

The activity of each catalyst was assessed by comparing the rate of guaiacol conversion normalized by the surface area and mass of the active phase (Figure 5). These measurements were carried out after 8 h TOS and at conversion levels between 27-75%. As such, the results do not necessarily reflect the intrinsic rates of each material. Instead, they allow for a comparative analysis of the catalysts at a single reaction condition relevant to *ex-situ* CFP. Although it is not directly investigated here, it has been reported that particle size effects can influence the activity and selectivity observed over supported transition metal catalysts [28, 29]. Given the variation in size of the active phase particles in this study, it is possible that particle size effects contribute to the differences in observed reactivity. In both cases, the Ni and Pt catalysts exhibited the highest rates of guaiacol conversion. On a per surface area basis, the com-Pt/SiO_2 catalyst was the most active, followed by NP-Ni/SiO_2, NP-Pt/SiO_2, and IW-Pt/SiO_2. Gravimetrically, IW-Pt/SiO_2 exhibited the highest rate, followed by NP-Ni/SiO_2, NP-Pt/SiO_2, and com-Pt/SiO_2. The observed lower activity of the metal phosphides relative to Pt catalysts is consistent with a previous report from Zhao, et al. [13]. It has been suggested that noble metals such as Pt facilitate C-O cleavage of aromatic oxygenates through a sequential hydrogenation-deoxygenation mechanism, which is more energetically favorable than direct deoxygenation of the aryl-OH bond (DDO) and may proceed at a faster rate [30]. It is noteworthy that based on active phase surface area, NP-Ni/SiO_2 and NP-Pt/SiO_2 exhibited higher rates of guaiacol conversion than IW-Ni/SiO_2 and IW-Pt/SiO_2 despite the presence of a ligand coating on the NP catalysts. It has been suggested that organic ligand modifiers can affect the activity and selectivity of heterogeneous catalyst systems by modifying the electronic environment of the catalyst, controlling the availability of specific active sites, and/or affecting the near-surface environment through interactions between the ligands and reagents [31-34]. The specific role of the surface ligands in this study remains unclear and further efforts are underway to better understand their effects.

The oxygen mol% of the organic phase and the product yield are presented in Figure 6. The products are grouped as containing zero oxygen atoms (cyclohexane, cyclohexene, benzene, and toluene), one oxygen atom (cyclopentanone, cyclohexanol, cyclohexanone, methoxycyclohexane, phenol, 2-methylphenol, 4-methylphenol, and anisole), and two oxygen atoms (2-hydroxycyclohexanone, 1,2-cyclohexanediol, 1-methyl-1,2-cyclohexanediol, 1,2-dimethoxybenzene, and 1,2-benzenediol). Despite exhibiting a lower total product yield than the Ni and Pt based catalysts, NP-Rh_2P/SiO_2 produced the highest yield of zero-oxygen products. NP-Ni/SiO_2, NP-Pt/SiO_2, and NP-Rh/SiO_2 also exhibited the production of zero-oxygen products, although to a lesser extent. The largest production of undesirable, two-oxygen products was observed over IW-Ni/SiO_2, com-Pt/SiO_2, and IW-Pt/SiO_2. These results are reflected in the magnitude of the oxygen mol% contained within the organic phase. The greatest reduction in oxygen mol% was observed over NP-Ni/SiO_2, which is consistent with its high total product yield and substantial production of one- and zero-oxygen products. A comparison of the Pt materials shows that NP-Pt/SiO_2 achieved the greatest reduction in oxygen mol% despite exhibiting a lower total product yield than the com or IW catalyst. This is due to the comparatively high yield of zero-oxygen products and low yield of two-oxygen products observed over the NP catalyst. The lowest reduction in oxygen mol% was observed over IW-Ni/SiO_2 which is consistent with its low total product yield and high production of two-oxygen products.

3.2.2 Product distribution

The experiments reported here were carried out at the same WHSV for all catalysts. Consequently, variability in the conversion must be considered when comparing product selectivity. This is particularly important for the deoxygenation of guaiacol, which has been proposed to occur in series with increased selectivity to deoxygenated and hydrogenated products at higher conversion [10,11,13]. In this study the product distribution provides insight into general trends, and comparisons between catalysts are

considered in the context of their relative conversion. The major products obtained over each catalyst are reported in Table 2. Minor products, which were obtained with less than 6% selectivity in all cases, are combined into a single category and classified as "other". These products include cyclohexene, toluene, methoxycyclohexane, 2-methylphenol, 4-methylphenol, 2-hydroxycyclohexanaone, 1,2-cyclohexanediol, 1-methyl-1,2-cyclohexanediol, 1,2-dimethoxybenzene, ethane, propane, butane, cyclopentane, and pentane. Phenol was formed with the highest selectivity over all of the catalysts except IW-Ni/SiO_2, which favored 1,2-benzenediol. The increased selectivity towards 1,2-benzenediol observed over IW-Ni/SiO_2 is consistent with its low guaiacol conversion, as 1,2-benzenediol has been identified as a primary product obtained during the deoxygenation of guaiacol [13]. The high selectivity to phenol, coupled with the production of methane and water, supports previous studies that suggest it can be formed in a two-step process from the deoxygenation of guaiacol over noble metal and metal phosphide catalysts under similar reaction conditions [10,11,13]. The first step involves hydrogenolysis of the methoxy methyl group to form 1,2-benzenediol and methane. This is followed by elimination of the remaining aryl-OH group as water viaDDO. However, it has also been proposed that phenol can be formed via direct demethoxylation to produce methanol [10,11,13]. It is possible that methanol is subsequently converted in a reverse methanol synthesis reaction to form carbon monoxide and hydrogen, which are thermodynamically favored at 350 °C.

The favorability of direct demethoxylation (to form phenol) compared to DDO (to form anisole) is related to the increased bond dissociation energy of the aryl-OH bond (468 kJ/mol) relative to the aryl-OR bond (422 kJ/mol) [35]. Despite being less energetically favorable, the production of anisole was observed over NP-Rh_2P/SiO_2 and NP-Ni_2P/SiO_2 with 19% and 9.3% selectivity, respectively. This is in contrast to the metallic catalysts, which exhibited less than 1.0% selectivity towards anisole. It has been proposed that on metal phosphide catalysts a charge transfer from the metal to the P atom imparts Lewis acidity to the metal site [36]. Given its electron deficiency, it is possible that the metal$^{\delta+}$ site forms stronger interactions with oxygen lone pair elections than a purely metallic site. This difference could facilitate DDO of the aryl-OH group and contribute to the higher selectivity towards anisole observed on the metal phosphide catalysts. In addition to its comparatively high selectivity towards anisole, NP-Rh_2P/SiO_2 demonstrated the highest combined selectivity to the deoxygenated products cyclohexane and benzene (26%). NP-Rh_2P/SiO_2 also demonstrated the lowest combined selectivity to 1-methyl-1,2-cyclohexanediol and 1,2-benezenediol (1.5%) which provide no deoxygentaion benefits, reduce carbon efficiency, and may contribute to catalyst deactivation [37]. These results, coupled with its ability to break aryl-OH bonds, suggest that NP-Rh_2P/SiO_2 may be a promising catalyst for the hydrodeoxygenation of pyrolysis vapor under *ex-situ* CFP conditions.

The production of cyclopentanone, which involves the elimination of a carbon atom within the ring structure of guaiacol, was observed over NP-Pt/SiO_2, IW-Pt/SiO_2, com-Pt/SiO_2, NP-Ni/SiO_2, IW-Ni/SiO_2 and NP-Rh/SiO_2. A previous study also identified the formation of cyclopentanone during the upgrading of guaiacol over Pt catalysts [38]. Although the precise route to the formation of this product is unknown, it has been proposed to proceed through a series of ring-opening and decarbonylation transformations.

At the elevated temperatures employed during *ex-situ* CFP (350-450 °C), the hydrogenation of aromatics and oxygenated aromatics is thermodynamically unfavorable [39], and correspondingly, the production of ring saturated products was limited over the catalysts explored here. However, cyclohexanone, cyclohexanol, and/or cyclohexane were observed to some extent over each catalyst. Ring hydrogenation was most favorable over NP-Ni/SiO_2, NP-Pt/SiO_2, IW-Pt/SiO_2, and com-Pt/SiO_2 (Table 3), suggesting that despite the thermodynamic limitations, the production of saturated products is possible under *ex-situ* CFP conditions and may be enhanced by the use of traditional hydrogenation catalysts. However, it should be noted that NP-Rh_2P/SiO_2 exhibited higher selectivity to cyclohexane (6.9%) than any other catalyst. The H/C ratio of the organic phase products provides a complementary measure of hydrogenation capability and addresses retention of the methoxy methyl group in addition to ring

hydrogenation (Table 3). The IW-Pt/SiO_2, com-Pt/SiO_2, NP-Pt/SiO_2, and NP-Ni/SiO_2 catalysts form products with the highest H/C ratio. Over these four catalysts, the H/C ratio of the organic phase was greater than or equal to 1.3, compared to an initial H/C ratio of 1.14 for guaiacol. The extent of hydrogenation was lowest on the metal phosphide catalysts. As discussed above, it is possible that the electrophilic metal site on the metal phosphide catalysts preferentially interacts with the oxygen lone pair elections, reducing the number of sites available for hydrogen activation.

The catalysts with the highest extent of hydrogenation also exhibited the greatest rate of guaiacol conversion (com-Pt/SiO_2, NP-Ni/SiO_2, NP-Pt/SiO_2, and IW-Pt/SiO_2). As discussed in Sec. 3.3.1, a sequential hydrogenation-deoxygenation mechanism is more energetically favorable than DDO and may proceed at a faster rate [30]. Given the increased selectivity towards hydrogenated products observed over the Pt and Ni catalysts in this study, it is possible that the sequential hydrogenation-deoxygenation pathway contributes to their enhanced activity. It should be noted that since ring hydrogenation is proposed to occur as a secondary reaction step during the deoxygenation of guaiacol, it is reasonable to suspect that extent of hydrogenation is affected by conversion [10, 11]. However, a comparion between NP-Ni/SiO_2, com-Pt/SiO_2, NP-Pt/SiO_2, and IW-Pt/SiO_2 shows that the Pt catalysts demonstrate a greater extent of hydrogenation despite exhibiting lower guaiacol conversion than NP-Ni/SiO_2. Consequently, it can be concluded that the extent of hydrogenation is not solely based on conversion and is affected by properties of the catalytic material.

3.2.3 Reaction pathways

A summary of the kinetically relevant transformations based on the observed product distributions is proposed in Figure 7. The formation of phenol is highly favorable on all of the catalysts and can occur through three different pathways, which are labeled in Figure 7. Pathway 1 is a likely route that involves demethylation to form 1,2-benzenediol and methane, followed by deoxygenation to phenol. This two-step sequence has been previously reported for the deoxygenation of guaiacol under low-pressure conditions and is supported by reports that identify 1,2-benzenediol as a primary reaction product [13,11,39]. Pathway 2 involves direct demethoxylation to produce methanol which can be subsequently converted to carbon monoxide. A comparison of the carbon selectivity to methane vs. methanol and carbon monoxide (Table 3) suggests that both pathways were active over all of the catalysts except IW-Ni/SiO_2 and NP-Ni_2P/SiO_2, which only produce methane. Among the catalysts that demonstrate both reaction pathways, the two-step sequence was favored by a ratio of at least 1.4:1 for all the materials except NP-Ni/SiO_2, which favored direct demethoxylation by a ratio of 7.8:1. Other studies have demonstrated that phenol can be formed from anisole with high selectivity over Pt/Al_2O_3 under similar reaction conditions [12]. As such, a separate two-step process in which guaiacol undergoes DDO to anisole followed by demethylation to phenol cannot be ruled out (pathway 3). Regardless of how it is formed, much of the phenol desorbs as a reaction product. However, some phenol is hydrogenated and/or deoxygenated to form a mixture of products including cyclohexane, cyclohexene, cyclohexanol, cyclohexanone, and benzene. Among these products, cyclohexane, cyclohexene, cyclohexanol, and cyclohexanone are favored relative to benzene for every catalyst except NP-Rh_2P/SiO_2, which favors benzene production with nearly a 2:1 molar ratio. This result, combined with its high selectivity towards anisole, suggests that NP-Rh_2P/SiO_2 is a promising catalyst for deoxygenation of aryl-OH bonds under *ex-situ* CFP conditions.

4. Conclusion

The metallic NP catalysts investigated in this study were more selective towards deoxygenated products than their IW and com analogues. The highest selectivity to completely deoxygenated products was observed over NP-Rh_2P/SiO_2, which to our knowledge has not been previously investigated for the deoxygenation of bio-oil model compounds under *ex-situ* CFP conditions. Compared to the other catalysts in this study, NP-Rh_2P/SiO_2 was particularly effective for deoxygenation of aryl-OH bonds, as

evidenced by its comparatively high selectivity to anisole and benzene. Although less selective towards deoxygenated products than the NP-Rh_2P/SiO_2 catalyst, NP-Ni/SiO_2 exhibited the largest reduction in the oxygen mol% of the organic phase and may offer a lower cost alternative. It is possible that the stabilizing ligands on the surface of the NP-catalysts contribute to their enhanced performance, and further efforts are underway to better understand how the ligands influence reactivity under *ex-situ* CFP conditions.

Acknowledgements:
This work was supported by the Department of Energy's Bioenergy Technology Office under Contract no. DE-AC36-08-GO28308.The authors wish to express thanks to Jesse Hensley for the valuable discussions, Jon Luecke for assistance with gas chromatography, Jason Thibodeaux for technical assistance in the laboratory, and Seth Noone for assistance with reactor operation and maintenance.

References:

1. Ruddy DA, Schaidle JA, Ferrell JR, Wang J, Moens L, Hensley JE (2014) Green Chemistry 16 (2):454-490
2. Kersten S, van Swaaij W, Lefferts L, Seshan K (2007) Catalysis for Renewables: From Feedstock to Energy Production. Wiley-VCH, Weinheim
3. Czernik S, Bridgwater AV (2004) Energy & Fuels 18 (2):590-598
4. Yaman S (2004) Energy Conversion and Management 45 (5):651-671
5. Mortensen PM, Grunwaldt JD, Jensen PA, Knudsen KG, Jensen AD (2011) Applied Catalysis A-General 407 (1-2):1-19
6. Bridgwater AV (2012) Environmental Progress & Sustainable Energy 31 (2):261-268.
7. Dutta A, Sahir A, Tan E, Humbird D, Snowden-Swan LJ, Meyer P, Ross J, Sexton D, Yap R, Lukas J (2015) Process Design and Economics for the Conversion of Lignocellulosic Biomass to Hydrocarbon Fuels: Thermochemical Research Pathways with *In Situ* and *Ex Situ* Upgrading of Fast Pyrolysis Vapors. U.S. Department of Energy Bioenergy Technologies Office
8. Venkatakrishnan VK, Delgass WN, Ribeiro FH, Agrawal R (2015) Green Chemistry 17 (1):178-183
9. Do PT, Foster AJ, Chen J, Lobo RF (2012) Green Chemistry 14 (5):1388-1397
10. Nimmanwudipong T, Runnebaum RC, Block DE, Gates BC (2011) Catalysis Letters 141 (6):779-783
11. Nimmanwudipong T, Runnebaum RC, Block DE, Gates BC (2011) Energy & Fuels 25 (8):3417-3427
12. Runnebaum RC, Nimmanwudipong T, Block DE, Gates BC (2011) Catalysis Letters 141 (6):817-820
13. Zhao HY, Li D, Bui P, Oyama ST (2011) Applied Catalysis A: General 391 (1–2):305-310
14. Phuong B, Antonio-Cecilia J, Oyama ST, Takagaki A, Infantes-Molina A, Zhao H, Li D, Rodriguez-Castellon E, Jimenez Lopez A (2012) Journal of Catalysis 294:184-198
15. Nie L, Resasco DE (2014) Journal of Catalysis 317:22-29
16. Boonyasuwat S, Omotoso T, Resasco DE, Crossley SP (2013) Catalysis Letters 143 (8):783-791
17. Oyama ST, Gott T, Zhao H, Lee YK (2009) Catalysis Today 143 (1–2):94-107
18. Li K, Wang R, Chen J (2011) Energy & Fuels 25 (3):854-863
19. Liu P, Rodriguez J (2003) Catalysis Letters 91 (3-4):247-252
20. Tao AR, Habas S, Yang P (2008) Small 4 (3):310-325
21. Jin RC (2012) Nanotechnology Reviews 1 (1):31-56
22. Ebitani K, Hattori H (1991) Bulletin of the Chemical Society of Japan 64 (8):2422-2427
23. Liu Z, Shamsuzzoha M, Ada ET, Reichert WM, Nikles DE (2007) Journal of Power Sources 164 (2):472-480
24. Carenco S, Boissière C, Nicole L, Sanchez C, Le Floch P, Mézailles N (2010) Chemistry of Materials 22 (4):1340-1349
25. Park KH, Jang K, Kim HJ, Son SU (2007) Angewandte Chemie-International Edition 46 (7):1152-1155.

26. Habas SE, Baddour FG, Ruddy DA, Nash CP, Pan M, Wang J, Hensley JE, Schaidle JA (2015) Chemistry of Materials, submitted
27. Rundqvist S (1960) Nature 185 (4705):31-32
28. Miller JT, Kropf AJ, Zha Y, Regalbuto JR, Delannoy L, Louis C, Bus E, van Bokhoven JA (2006) Journal of Catalysis 2 (10): 222-234
29. Melaet G, Lindeman AE, Somorjai, GA (2014) Topics in Catalysis 57 (6-9): 500-507
30. Wang HM, Male J, Wang Y (2013) ACS Catalysis 3 (5):1047-1070
31. Pang SH, Schoenbaum CA, Schwartz DK, Medlin JW (2014) ACS Catalysis 4 (9):3123-3131.
32. Pang SH, Schoenbaum CA, Schwartz DK, Medlin JW (2013) Nature Communications 4: 2448
33. Schoenbaum CA, Schwartz DK, Medlin JW (2014) Accounts of Chemical Research 47 (4):1438-1445
34. Pang SH, Love NE, Medlin JW (2014) Journal of Physical Chemistry Letters 5 (23):4110-4114
35. Furimsky E (2000) Applied Catalysis A-General 199 (2):147-190
36. Liu P, Rodriguez JA, Asakura T, Gomes J, Nakamura K (2005) Journal of Physical Chemistry B 109 (10):4575-4583
37. Ghampson IT, Sepulveda C, Garcia R, Fierro JL, Escalona N, DeSisto WJ (2012) Applied Catalysis A-General 435:51-60
38. Nimmanwudipong T, Aydin C, Lu J, Runnebaum RC, Brodwater KC, Browning ND, Block DE, Gates BC (2012) Catalysis Letters 142 (10): 1190-1196
39. Lu JM, Behtash S, Mamun O, Heyden A (2015) ACS Catalysis 5 (4):2423-2435

Figures

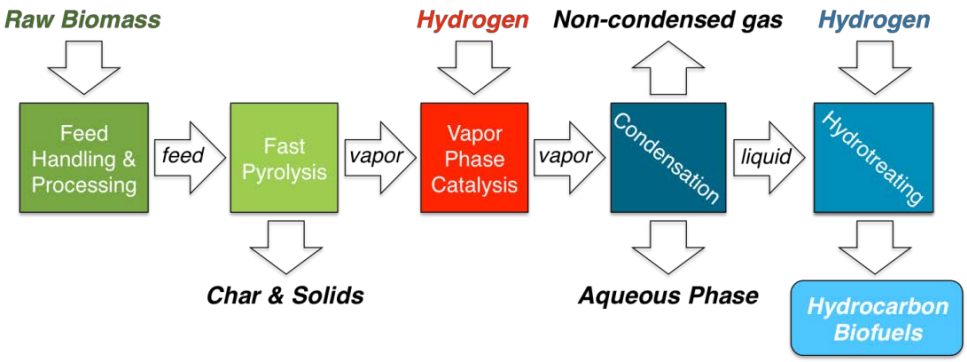

Figure 1: Process block flow diagram for *ex-situ* CFP. Adapted from reference [1].

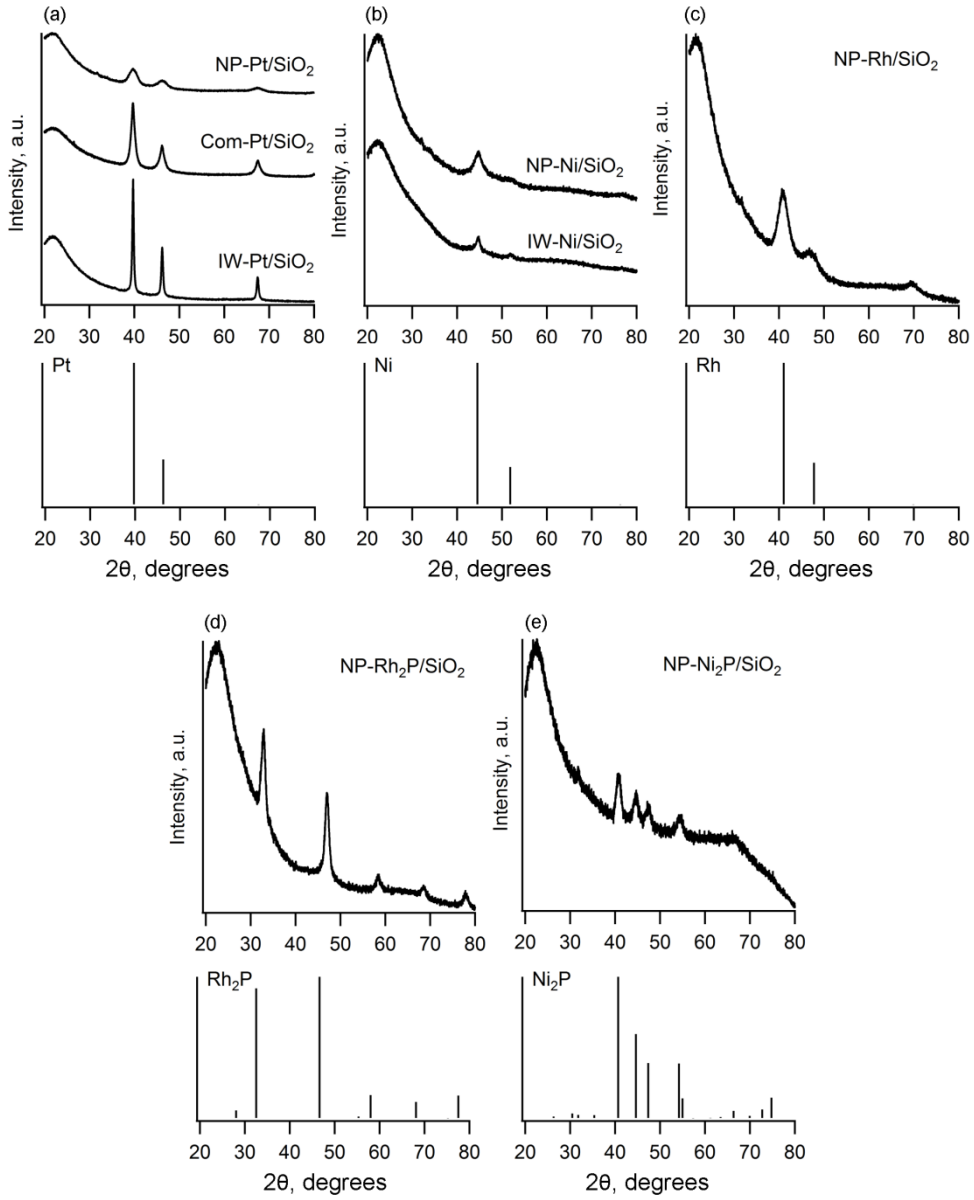

Figure 2: XRD patterns of (a) Pt, (b) Ni, (c) Rh, (d) Rh_2P, and (e) Ni_2P materials supported on SiO_2. Reference diffraction patterns are included for comparison.

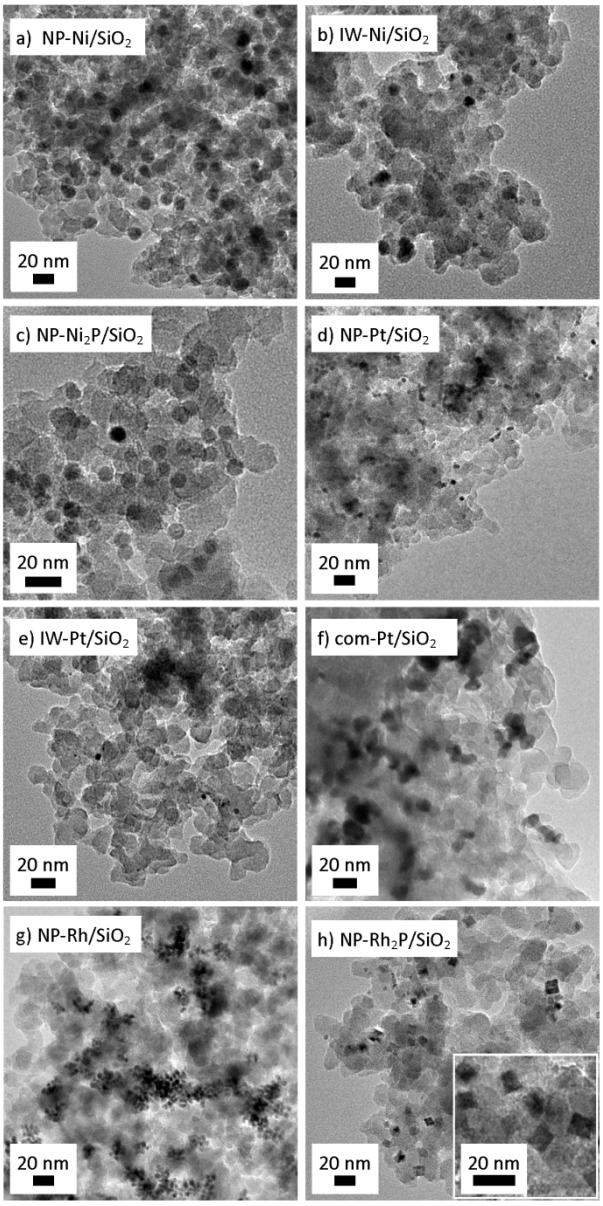

Figure 3: TEM images of a) NP-Ni/SiO_2, b) IW-Ni/SiO_2, c) NP-Ni_2P/SiO_2, d) NP-Pt/SiO_2, e) IW-Pt/SiO_2, f) com-Pt/SiO_2, g) NP-Rh/SiO_2, and h) NP-Rh_2P/SiO_2.

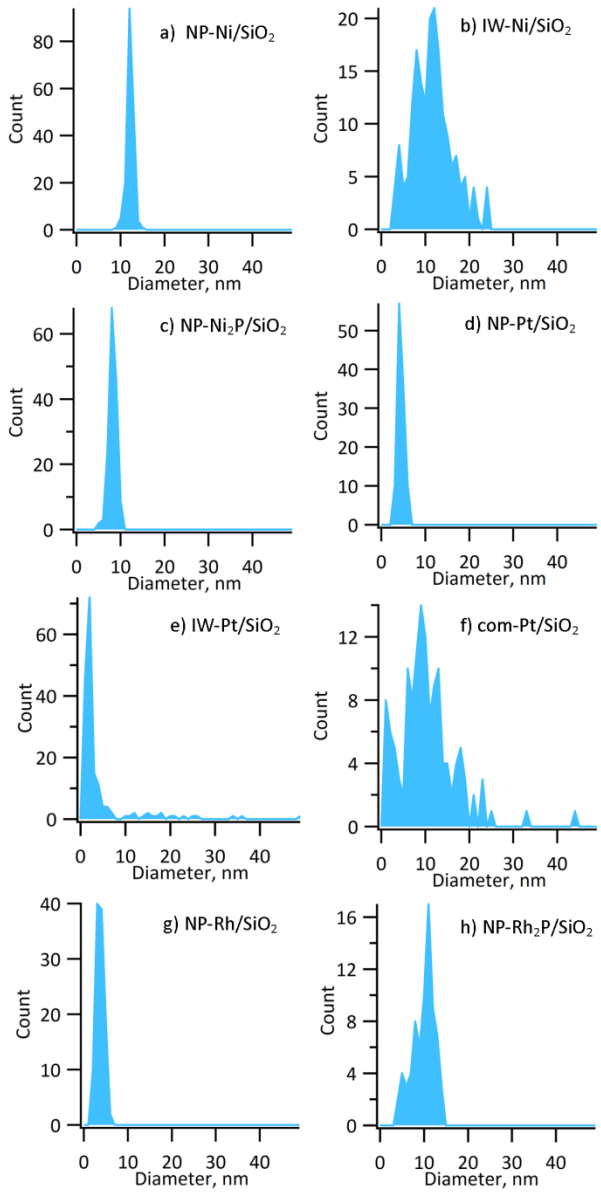

Figure 4: Particle size distribution obtained from TEM images for a) NP-Ni/SiO_2, b) IW-Ni/SiO_2, c) NP-Ni_2P/SiO_2, d) NP-Pt/SiO_2, e) IW-Pt/SiO_2, f) com-Pt/SiO_2, g) NP-Rh/SiO_2, and h) NP-Rh_2P/SiO_2.

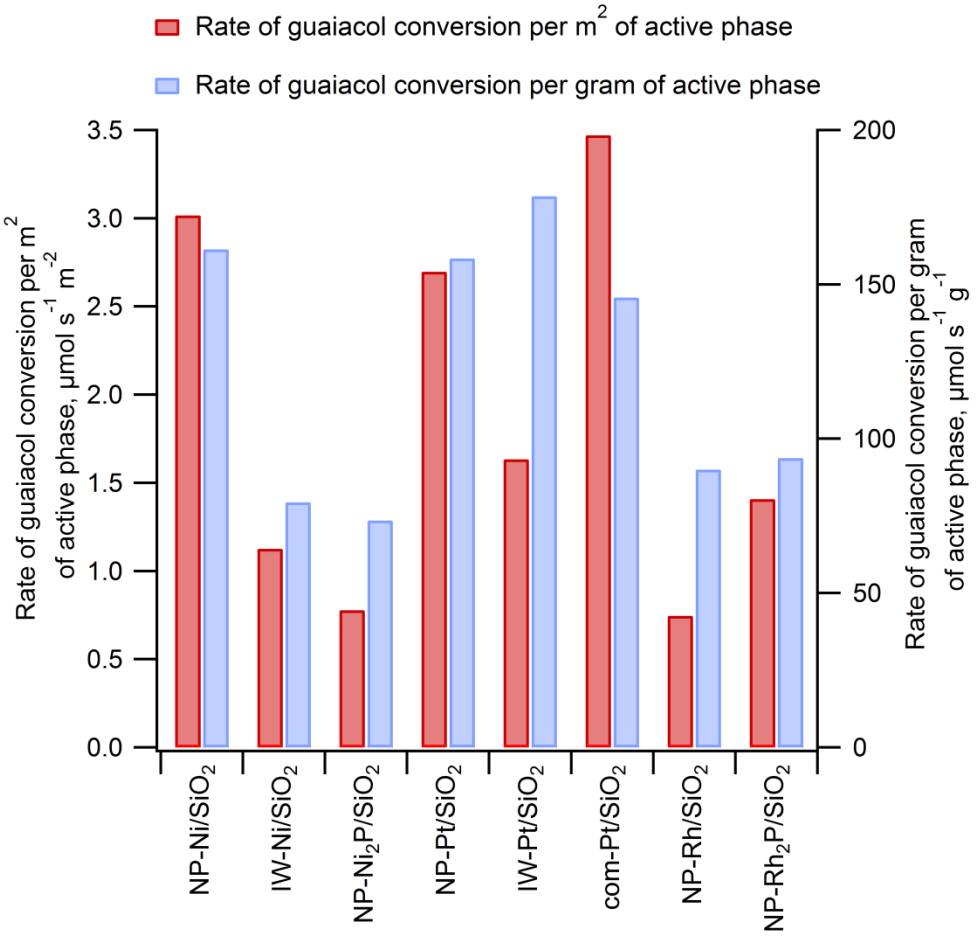

Figure 5: The normalized rate of guaiacol conversion per m^2 of active phase surface area and per gram of active phase mass observed during the hydrodeoxygenation of guaiacol under *ex-situ* CFP conditions (350 °C, 0.5 MPa, 12 H_2:1 guaiacol, WHSV 5 h^{-1}). Data points were collected at 8 h TOS.

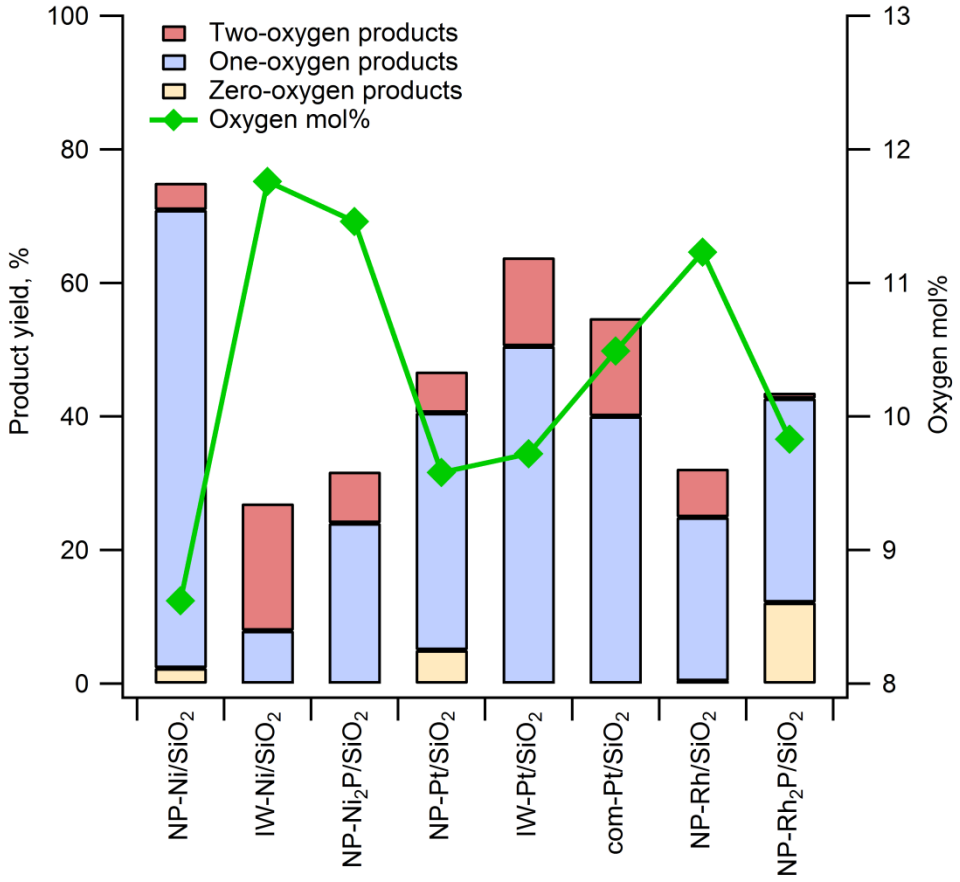

Figure 6: Product yield and oxygen mol% contained within the organic phase obtained during the hydrodeoxygenation of guaiacol under *ex-situ* CFP conditions (350 °C, 0.5 MPa, 12 H_2:1 guaiacol, WHSV 5 h^{-1}). Guaiacol has an initial oxygen mol% of 11.8%. Data points were collected at 8 h TOS.

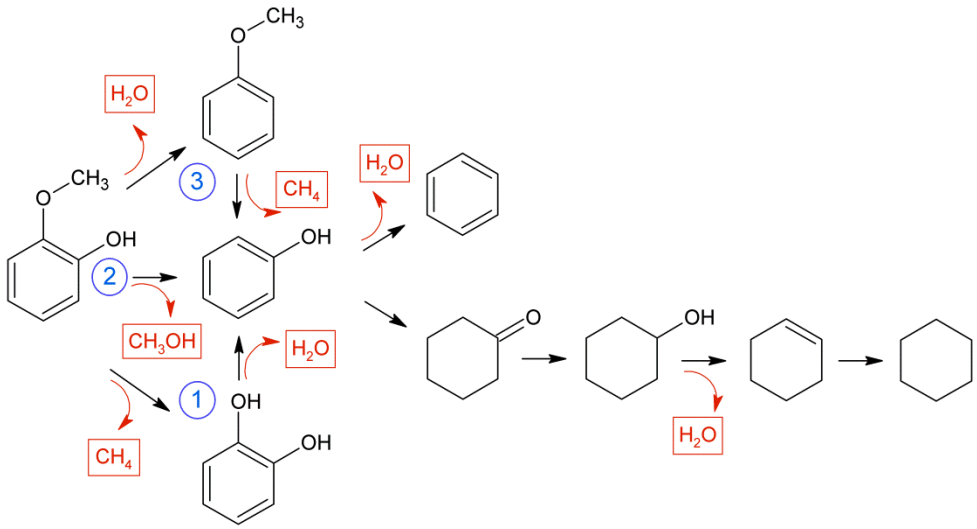

Figure 7: A summary of the common transformations observed during the hydrodeoxygenation of guaiacol under *ex-situ* CFP conditions based on observations from this work and references in Ruddy, et al. [1]. Specific pathways are numbered and referenced in the text.

Table 1: Active phase loading, crystallite size, average particle diameter, particle geometry, and active phase surface area of each catalyst.

Catalyst	Active phase loading (wt%)	Crystallite size from XRD (nm)	Average diameter from TEM (nm)[a]	Particle geometry from TEM	Active phase surface area ($m^2 g^{-1}$)[b]
NP-Ni/SiO_2	5.2	3.5	13.0 ± 0.8	Spherical	2.8
IW-Ni/SiO_2	3.8	7.8	11 ± 5	Spherical	2.7
NP-Ni_2P/SiO_2	4.8	7.8	8.7 ± 0.9	Spherical	4.6
NP-Pt/SiO_2	3.3	3.4	4.9 ± 0.7	Spherical	1.9
IW-Pt/SiO_2	4.0	23	5 ± 7	Spherical	4.4
com-Pt/SiO_2	4.2	7.3	11 ± 6	Spherical	1.8
NP-Rh/SiO_2	4.0	3.0	4.2 ± 0.9	Spherical	4.8
NP-Rh_2P/SiO_2	5.2	8.5	10 ± 3	Cubic	3.5

a) Reported range represents ± one standard deviation. b) Calculated based on the particle size distribution and geometry obtained from TEM.

Table 2: Conversion, organic phase selectivity, and byproduct selectivity observed during the hydrodeoxygenation of guaiacol under *ex-situ* CFP conditions (350 °C, 0.5 MPa, 12 H_2:1 guaiacol, WHSV 5 h^{-1}, data collected at 8 h TOS).

	NP-Ni	IW-Ni	NP-Ni_2P	NP-Pt	IW-Pt	com-Pt	NP-Rh	NP-Rh_2P
Conversion	75	27	32	47	64	55	32	44
	Organic phase selectivity							
Cyclohexane	1.1	-	-	2.4	-	-	-	6.9
Benzene	1.7	-	-	6.7	-	-	-	19
Cyclopentanone	0.41	0.37	-	6.4	14	8.1	1.7	-
Cyclohexanol	9.7	0.85	2.0	9.3	5.8	3.6	3.5	0.31
Cyclohexanone	17	3.2	5.0	15	17	12	10	0.78
Phenol	63	23	58	42	42	49	59	49
Anisole	0.97	0.45	9.3	0.39	0.25	0.12	0.69	19
1-methyl-1,2-cyclohexanediol	4.9	11	8.8	2.4	5.3	6.7	3.4	0.34
1,2-benzenediol	0.37	54	14	9.4	9.3	15	17	1.1
Other	0.83	8.3	3.1	5.3	6.5	6.0	3.9	3.4
	Byproduct selectivity							
Methanol	44	-	-	8.6	-	-	-	26
Methane	11	100	80	52	54	58	65	45
Water	3.4	-	20	9.1	6.0	6.4	1.8	22
Carbon monoxide	42	-	-	30	36	30	27	6.5
Other	-	-	-	-	4.1	5.3	5.3	-

Table 3: Selectivity ratios for various product classes obtained during the hydrodeoxygenation of guaiacol under ex-situ CFP conditions (350 °C, 0.5 MPa, 12 H_2:1 Guaiacol, WHSV 5 h^{-1}, data collected at 8 h TOS).

Catalyst	Ratio of ring hydrogenated to aromatic products[a]	Ratio of hydrogen to carbon[a,b]	Ratio of methane to carbon monoxide + methanol
NP-Ni/SiO_2	0.50	1.3	0.13
IW-Ni/SiO_2	0.25	1.2	Only Methane
NP-Ni_2P/SiO_2	0.19	1.2	Only Methane
NP-Pt/SiO_2	0.64	1.3	1.4
IW-Pt/SiO_2	0.94	1.4	1.5
com-Pt/SiO_2	0.56	1.3	2.0
NP-Rh/SiO_2	0.26	1.2	2.4
NP-Rh_2P/SiO_2	0.11	1.1	1.4

a) Contained within the organic phase. b) Guaiacol has an initial H/C ratio of 1.14.